

FREE-MOLECULAR FLOW INDUCED ATTITUDE CHANGES OF SPINNING SATELLITES IN ELLIPTICAL ORBITS

Jozef C. van der Ha*

This paper presents a method for obtaining the attitude changes experienced by a spinning satellite under torques induced by free-molecular flow. The results are relevant for objects in elliptical Earth orbits with perigees below about 600 km. In particular, this includes satellites and rocket bodies in geostationary transfer orbits. First, a few fundamental aspects of free-molecular flow interactions with satellite surfaces are presented, e.g. the momentum exchanges originating from Maxwell-Boltzmann's kinetic gas theory. Expressions for the forces and torques acting on typical spinning satellite configurations are given. The average change in the attitude pointing over a spin revolution is established by integrating the torque vector over the perigee region. The integral is evaluated in the form of an asymptotic series expansion. Its leading term is an analytical expression in terms of the orbital elements, the angle between velocity vector and spin-axis, the air density and scale height values, the satellite's geometrical parameters, and the coefficients modeling the molecular flow and satellite surface interactions.

INTRODUCTION

This paper studies the attitude changes experienced by spinning satellites or rocket bodies under torques induced by free-molecular flow (FMF). The results are relevant for satellites in elliptical orbits with perigees below about 600 km. In particular, this includes communications and weather satellites launched into Geostationary Transfer Orbits (GTO's) prior to their solid- or liquid-motor injections into Geostationary Orbit (GEO). The results are also of practical interest for predicting the attitude evolutions of spinning launcher stages that are discarded in GTO or in other elliptical trajectories after injecting their payloads.

The study of free-molecular flow interactions with satellite surfaces dates back to the early 1960's. For example, Schaaf and Chambre¹ present effective models based on accommodation coefficients for energy and momentum exchanges between the incident atmospheric molecules and satellite surfaces. These results have been used for calculating drag coefficients of a number of different satellite configurations under low-Earth-orbit conditions, see Cook².

During the 1980's, Koppenwallner³ and his co-workers⁴⁻⁶ established analytical and numerical models for calculating the forces and torques induced by the free-molecular flow on the basis of Maxwell-Boltzmann's kinetic gas theory. These models have been applied successfully for the evaluation of the forces and torques acting on actual in-flight ESA satellite configurations like TD-1A⁴ and MARECS-A⁵ by means of comprehensive numerical simulations. Furthermore, wind tunnel tests have been conducted⁶ to reproduce the observed attitude changes of the MARECS-A satellite during its three GTO perigee passages.

* Consultant, 5808 Bell Creek Rd, Deming, WA 98244, USA; JvdHa@aol.com.

A useful analytical model for predicting the attitude changes resulting from free-molecular effects on a few realistic satellite configurations has been developed by the author⁷ in the early 1980's. This study had been triggered by unexpected attitude changes of about 0.05° experienced by the ESA-operated satellite MARECS-A satellite during its GTO perigee passages in December 1981. The analytical results⁸ demonstrated convincingly that the observed attitude changes were indeed caused by the free-molecular flow torques in the perigee region.

The present paper first summarizes a few of the fundamental aspects of free-molecular flow interactions with satellite surfaces. This includes the normal and tangential momentum transfer associated with the molecular velocity distributions predicted by Maxwell-Boltzmann's kinetic gas theory. A large fraction of the incident molecules are accommodated or adsorbed by the satellite surface and are subsequently re-emitted at the molecular velocity associated with the surface temperature. A smaller fraction of the molecules are reflected specularly off the surface.

The resulting forces are calculated from the momentum exchanges and are expanded in normal and tangential components relative to the satellite surface under consideration. Also the familiar drag and lift coefficients follow directly from this formulation. Detailed expressions for the forces and torques acting on a few basic satellite surface configurations are established. These results form the basis for predicting the forces and torques acting on representative satellite configurations, in particular the cylindrical and box-like types.

Of particular interest is a generic expression for the free-molecular torque that covers, at least in principle, any symmetrical satellite geometrical configuration. This torque expression depends on the orbital velocity vector and the satellite spin axis direction in inertial space as well as environmental parameters like the local density and scale height values, the free-molecular flow characteristics expressed by the diffuse reflectivity parameter, the velocities of the incident and reflected molecules, and finally the satellite's geometrical parameters and center of mass location.

Typical elliptical orbits that are used for many low-Earth mission applications have relatively large $\beta = ae/H_p$ values, where a denotes the semi-major axis, e is the eccentricity, and H_p stands for the density scale height at perigee (for example, GTO's have $\beta \approx 500$). As a consequence, the FMF forces and torques predominantly originate in the region very close to the perigee position. Therefore, it is justified to expand the exponential density model in terms of an asymptotic power series in the eccentric anomaly. The results indicate that, for a typical GTO, the 1 % threshold level of the density value at the perigee is already reached at eccentric anomalies of $\pm 7.5^\circ$. Consequently, the forces and torques induced by the density effects are essentially negligible beyond an interval of about 7 minutes centered on the perigee position.

The integrated torque over the perigee region corresponds to the change in the spin angular momentum vector, which equals the change in the spin-axis attitude after nutation effects have subsided. A practically useful expression for the attitude change is established in terms of a power series in the small parameter $1/\beta = H_p/(ae)$ and its geometrical implications are analyzed.

Simulations have been performed to improve our understanding of the dependence of the resulting attitude change on the input parameters. In particular, this concerns the perigee altitude, the semi-major axis, the orientation of the satellite spin axis relative to the orbit velocity vector at perigee, the density and scale height values, the satellite geometrical configuration properties, and the free-molecular accommodation coefficients. The magnitude of the attitude change depends very strongly on the perigee altitude. The maximum possible attitude change ranges from about 0.1° at a perigee of 200 km to about 4.8° for a perigee of 150 km (under identical density values).

The influence of the air density variations on the induced attitude changes is also investigated and we find that the magnitude of the resulting attitude changes may vary by a factor of about 3.

FREE-MOLECULAR FLOW

Free-molecular flow (FMF) refers to a free stream of molecules that have a mean free path λ_0 that is large compared to a typical satellite linear dimension L , see Cook², p. 929. Therefore, the Knudsen number $K = \lambda_0/L$ should be much larger than 1. The free stream number density is n_0 and the molecules impinge on the body with speed v_i so the number of molecules arriving at a unit projected surface area in unit time is $n_0 v_i$. In practice, the free-stream molecular velocity v_i may be taken equal to the satellite's orbital velocity v but with the opposite direction.

Because most molecules are re-emitted from the satellite surface (or 'wall') at a speed $v_w < v_i$, the number density of the re-emitted molecules near the surface is larger than n_0 , i.e. of the order of $n_0 v_i / v_w$. Since the mean free path is inversely proportional to the density, the mean free path of the incident molecules near the surface becomes $\lambda = \lambda_0 v_w / v_i (< \lambda_0)$. Therefore, for a body moving at high incident velocity, the condition $K > 1$ may not be sufficient to ensure FMF if the surface temperature is low and if appreciable adsorption of the molecules takes place at the satellite surface. A more meaningful requirement for FMF may thus be expressed by the condition:

$$K = \lambda/L = \lambda_0 v_w / (L v_i) \gg 1 \rightarrow \lambda_0 / L \gg v_i / v_w > 1 \quad (1a,b)$$

In practice, we have $v_i/v_w \approx 13$ if the molecules are re-emitted with a speed corresponding to the surface temperature of 300 °K. For instance, at altitudes of 160 / 200 / 250 km, the mean free paths are at least 60 / 200 / 630 m, respectively, see Cook², Figure 1. Thus, satellites that are launched into orbits with perigees at these altitudes are expected to experience FMF interactions.

An important parameter for describing the drag coefficient of a satellite in a free-molecular flow environment is the *molecular speed ratio* $S = v/v_m$, i.e. (satellite's orbital velocity v) / (most probable molecular speed v_m). The most probable molecular velocity v_m at an arbitrary altitude follows from Maxwell-Boltzmann's kinetic gas theory and is given by (see Cook², Eq. 3):

$$v_m = \sqrt{(2RT_m/M)} = \sqrt{2Hg} \quad (2)$$

where T_m is the *atmospheric* or *ambient* temperature at the location of the molecules, M is the molecular mass, R the universal gas constant, H is the scale height, and g is the local gravity acceleration. The main atmospheric constituents in the Earth's atmosphere are N_2 , O_2 , O , He , Ar , and H . Atomic oxygen is most prominent over the altitude range between 150 and 800 km.

The molecular velocity v_m increases from about 700 m/s at 150 km altitude to about 1.5 km/s at 700 km height (see Cook², p. 931). Because the satellite's velocity is always higher than 7.5 km/s at these altitudes, we find that $v_i/v_m > 5$ throughout the range of altitudes from 150 to 700 km. Under these conditions, the flow in this region is called *hyper-thermal*, which indicates that the errors induced by neglecting the random thermal motion of the atmospheric molecules may well be acceptable in practical FMF applications.

The interactions of the free-flow molecules with the satellite surface depend on the surface characteristics and are complicated. The energy accommodation coefficient α is used^{1,2} to express the ratio of the energy change of the incident molecules relative to the maximum possible change (i.e., when the accommodation were perfect). When introducing the average incident molecular kinetic energy E_i , the average reflected energy E_r , and the average energy of re-emitted molecules E_w (associated with velocity v_w and surface temperature T_w), α is expressed by:

$$\alpha = (E_i - E_r) / (E_i - E_w) \quad (3)$$

Furthermore, the following velocity ratios follow from the molecular kinetic energies:

$$v_r/v_i = \sqrt{(E_r/E_i)}; \quad v_w/v_i = \sqrt{(E_w/E_i)} \quad (4a,b)$$

AERODYNAMIC FORCE MODEL

Aerodynamic effects are the dominant non-gravitational forces acting on an Earth-orbiting satellite below 600 km altitude. The dynamics of the neutral upper atmosphere are governed by complex physical interactions as explained, for instance, in References 9 and 10. These processes are mainly driven by the Sun's extreme ultra-violet (EUV) radiation, which is well correlated with the 10.7 cm solar flux and can in fact be measured on Earth (i.e., the well-known F_{10.7} index).

Here, we use the FMF aerodynamic model presented by Klinkrad and Fritzsche⁹, who express the aerodynamic force \mathbf{F} exerted on a flat satellite surface A in the form:

$$\mathbf{F} = \frac{1}{2} \rho A v_i^2 \mathbf{C} \quad (5)$$

The local atmospheric density ρ (in units of kg/m³) follows from the summation of the concentration profiles of the n dominant atmospheric constituents (e.g., N₂, O₂, O, He, Ar, H, N):

$$\rho = \sum_{j=1}^n (\rho_j) \quad (6)$$

The respective scale heights associated with the n constituents are proportional to the quotient of the constituents' molecular mass and ambient temperature. Thus, heavier molecules such as N₂ and O dominate at lower altitudes (below 400 km) and the lighter molecules He, H at higher altitudes and into the exosphere.

The remaining parameters appearing in Eq. (5) are defined as follows: the area A in m² may be an actual flat surface element or a representative flat satellite cross-sectional area of the satellite; v_i is the free-stream incident velocity in m/s. Finally, the non-dimensional vector coefficient \mathbf{C} contains the satellite characteristics (e.g., detailed geometrical configuration, accommodation characteristics, and attitude relative to the flow) affecting the aerodynamic force. The vector \mathbf{C} may be interpreted as a short-hand representation of the aerodynamic *drag* and *lift* coefficients.

The calculation of the aerodynamic forces requires understanding of the intricate interactions of the incident molecules with the satellite surfaces exposed to the flow. These may be modeled by the accommodation coefficient α in Eq. (3). An alternative, although equivalent, approach is adopted here. A fraction of the molecules is assumed to be reflected *specularly*, i.e. an elastic reflection off the surface with momentum transfer occurring only in the surface-normal direction. The remaining molecules are adsorbed by the surface and may experience a number of collisions with the surface molecules before being re-emitted in an arbitrary direction, i.e. *diffusely*. The force induced by the diffuse re-emission acts also normal to the surface. In this case, however, a tangential force component is generated by the momentum transfer due to the adsorption of the incident molecules (provided that the direction of incidence is *not* normal to the surface).

The fraction of the incident molecules that is reflected *diffusely* is denoted by σ_d (with $0 \leq \sigma_d \leq 1$). The nature of the re-emission will be assumed to be in accordance with Lambert's cosine law, see Figure 1. These molecules lose almost all of their momentum when they are accommodated on the surface. Subsequently, they will be emitted diffusely with the most probable velocity v_w corresponding to the Maxwell-Boltzmann velocity distribution that is associated with the surface temperature T_w . The recoil force resulting from the re-emission acts *normal* to the surface area in the direction of its (inward) normal vector \mathbf{n} as illustrated by the geometry in Figure 1.

The relationship between the unit-vectors \mathbf{u} , \mathbf{n} , and \mathbf{t} follows from the geometry in Figure 1:

$$\mathbf{u} = \cos \vartheta \mathbf{n} + \sin \vartheta \mathbf{t} \quad (7)$$

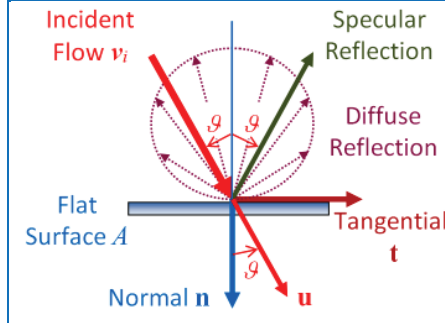


Figure 1. Illustration of Diffuse and Specular Reflections and Definitions of Unit-Vectors \mathbf{u} , \mathbf{n} , \mathbf{t} .

The non-diffusely reflected fraction ($1-\sigma_d$) is reflected specularly as shown in Figure 1. These molecules are *not* at all accommodated by the surface and they preserve their incoming tangential velocity components. Thus, there is no exchange of tangential momentum (Note: the incidence and reflection angles are identical and equal to ϑ). However, the velocity components normal to the surface change signs during the reflection off the surface thereby creating a recoil force (in the normal direction) of the same magnitude as the force induced by the incident molecules.

In conclusion, the coefficient \mathbf{C} in Eq. (5) may be split up in diffuse and specular parts:

$$\mathbf{C} = \sigma_d \mathbf{c}_d + \sigma_s \mathbf{c}_s; \quad \text{with: } \sigma_s = 1 - \sigma_d \quad (8)$$

with \mathbf{c}_d and \mathbf{c}_s representing the diffuse and specular momentum interactions with the surface A , respectively. As indicated already, the coefficient \mathbf{c}_d has components normal and tangential to the satellite surface, whereas \mathbf{c}_s contributes only a component along the normal direction \mathbf{n} .

Practically useful free-molecular force models can be established from Maxwell-Boltzmann's kinetic theory of gases. This involves the use of the *pressure* and *particle flux* functions Π and χ , see for instance Koppenwallner³. This leads to the following expressions for the coefficients \mathbf{c}_d and \mathbf{c}_s in terms of the wall temperature T_w and the ambient atmospheric temperature T :

$$\mathbf{c}_d = \left(\frac{v_m}{v_i} \right)^2 \left\{ \left(\frac{\Pi(S_n)}{\sqrt{\pi}} + \frac{1}{2} \sqrt{\frac{T_w}{T_m}} \chi(S_n) \right) \mathbf{n} + \left(\frac{S_t \chi(S_n)}{\sqrt{\pi}} \right) \mathbf{t} \right\} \quad (9a)$$

$$\mathbf{c}_s = \frac{2}{\sqrt{\pi}} \left(\frac{v_m}{v_i} \right)^2 \Pi(S_n) \mathbf{n} \quad (9b)$$

with:

$$\Pi(S_n) = S_n \exp(-S_n^2) + \sqrt{\pi} (S_n^2 + 0.5) \{1 + \text{erf}(S_n)\} \quad (10a)$$

$$\chi(S_n) = \exp(-S_n^2) + \sqrt{\pi} S_n \{1 + \text{erf}(S_n)\} \quad (10b)$$

$$S_n = (v_i / v_m) \cos \vartheta; \quad S_t = (v_i / v_m) \sin \vartheta \quad (10c,d)$$

$$\sqrt{(T_w / T_m)} = v_w / v_m \quad (10e)$$

If S_n is sufficiently large Eqs. (10a,b) may be simplified as follows (errors $< 10^{-6}$ for $S_n > 3.5$):

$$\Pi(S_n) \approx \sqrt{\pi} (2S_n^2 + 1); \quad \chi(S_n) \approx 2\sqrt{\pi} S_n \quad (11a,b)$$

Although the velocity ratio $v_i/v_m > 5$ for altitudes above 150 km, the validity of the approximate results in Eqs. (11) breaks down when ϑ comes within a few degrees of 90° due to the cosine term in Eq. (10c). On the other hand, the incidence angle with respect to the surface is shallow here so that the force is relatively small in any case and the induced errors are immaterial.

The approximations in Eqs. (11) lead to more straightforward results for Eqs. (9a,b):

$$\begin{aligned}\mathbf{c}_d &\equiv \left(\frac{v_m}{v_i} \right)^2 \left\{ \left[2S_n^2 + 1 + \sqrt{\pi} S_n \left(\frac{v_w}{v_m} \right) \right] \mathbf{n} + 2S_t S_n \mathbf{t} \right\} = \\ &= \left\{ 2 \cos^2 \vartheta + \left(\frac{v_m}{v_i} \right)^2 + \sqrt{\pi} \left(\frac{v_w}{v_i} \right) \cos \vartheta \mathbf{n} + \sin(2\vartheta) \mathbf{t} \right\};\end{aligned}\quad (12a)$$

$$\mathbf{c}_s \equiv 2 \left\{ 2 \cos^2 \vartheta + \left(\frac{v_m}{v_i} \right)^2 \right\} \mathbf{n} \quad (12b)$$

The aerodynamic vector-coefficient \mathbf{C} in Eq. (8) can now be expressed as:

$$\begin{aligned}\mathbf{C} &= \left\{ (2 - \sigma_d) \left(2 \cos^2 \vartheta + \left(\frac{v_m}{v_i} \right)^2 \right) + \sigma_d \sqrt{\pi} \left(\frac{v_w}{v_i} \right) \cos \vartheta \right\} \mathbf{n} + \sigma_d \sin(2\vartheta) \mathbf{t} \Rightarrow \\ \mathbf{C} &= C_n \mathbf{n} + C_t \mathbf{t}\end{aligned}\quad (13)$$

with the scalar FMF parameters C_n and C_t defined by:

$$C_n = c_0 + c_1 \cos \vartheta + c_2 \cos^2 \vartheta; \quad C_t = \sigma_d \sin(2\vartheta) \quad (14a,b)$$

and:

$$c_0 = (2 - \sigma_d) \left(\frac{v_m}{v_i} \right)^2; \quad c_1 = \sigma_d \sqrt{\pi} \left(\frac{v_w}{v_i} \right); \quad c_2 = 2(2 - \sigma_d) \quad (15a-c)$$

These results may be interpreted physically as follows: c_0 is the normal momentum transfer due to the thermal speeds of the incident and specularly reflected molecules; c_1 is the normal momentum transfer of molecules that are diffusely re-emitted at surface temperature (after accommodation); c_2 is the normal momentum transfer due to the velocities of the incident and specularly reflected molecules. Finally, the parameter C_t expresses the transfer of tangential momentum by the incident molecules that are accommodated on the surface.

Figure 2 illustrates the behavior of the FMF coefficients C_n and C_t as functions of ϑ for three different values of σ_d in the range from 0.9 to 1.0. (It is known that $\sigma_d > 0.95$ at about 200 km¹¹.) Additional inputs that are needed here are $T_w/T \cong 0.3$ and $v_i/v_m \cong 10$. Figure 2 shows that the variations of C_n and C_t for different σ_d values stay within about 10 % of the results for $\sigma_d = 1$. The results hardly change when different v_m/v_i ratios are used. This is because of the large differences in the magnitudes of the parameters defined in Eqs. (15), i.e. $c_2 \cong 25 \times c_1$ and $c_1 \cong 8 \times c_0$.

The familiar *drag* and *lift* coefficients C_D and C_L follow from Eqs. (13-14), see also Figure 1:

$$\begin{pmatrix} C_D \\ C_L \end{pmatrix} = \begin{bmatrix} \cos \vartheta & \sin \vartheta \\ -\sin \vartheta & \cos \vartheta \end{bmatrix} \begin{pmatrix} C_n \\ C_t \end{pmatrix} \quad (16)$$

The magnitude of C_L is relatively small for satellite applications, i.e. typically below 10 % of C_D .

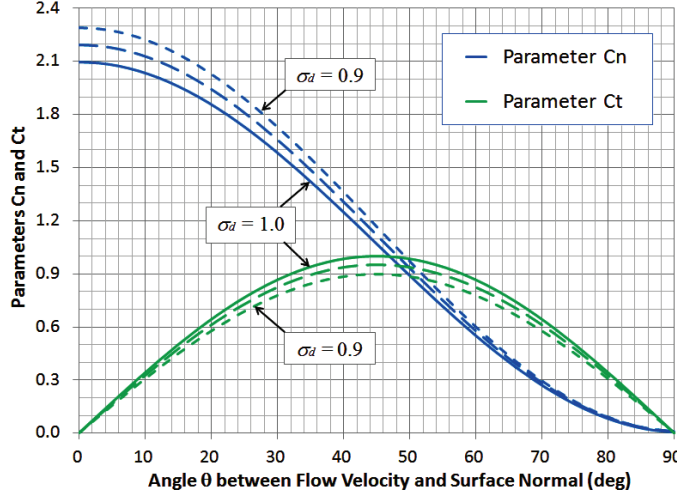


Figure 2. Parameters C_n and C_t as Functions of ϑ for $\sigma_d = 0.9, 0.95, 1.0$.

Finally, we mention that the satellite spin motion induces an additional tangential momentum transfer due to the FMF molecules interactions with the external surfaces. Considering a 60-rpm spin rate and a 1-m satellite radius, the inertial speed of the satellite's outer surface would be 2π m/s, i.e. < 0.1 % of the orbital speed v . Although the magnitude of the resulting force is negligible compared to the FMF forces presented above, its effect is very different, namely a spin-down.

In this connection, we mention that the inertial equatorial velocity of the Earth's co-rotating atmosphere is about 465 m/s, which is 4.3 % of the GTO perigee velocity and is considerably higher than the spin effect. Also this effect is not taken into consideration here.

FORCE AND TORQUE EXPRESSIONS

The results of Eqs. (5) and (13) indicate that the FMF force acting on an arbitrary flat plate can be written in its components along the normal and tangential directions, see also Figure 1:

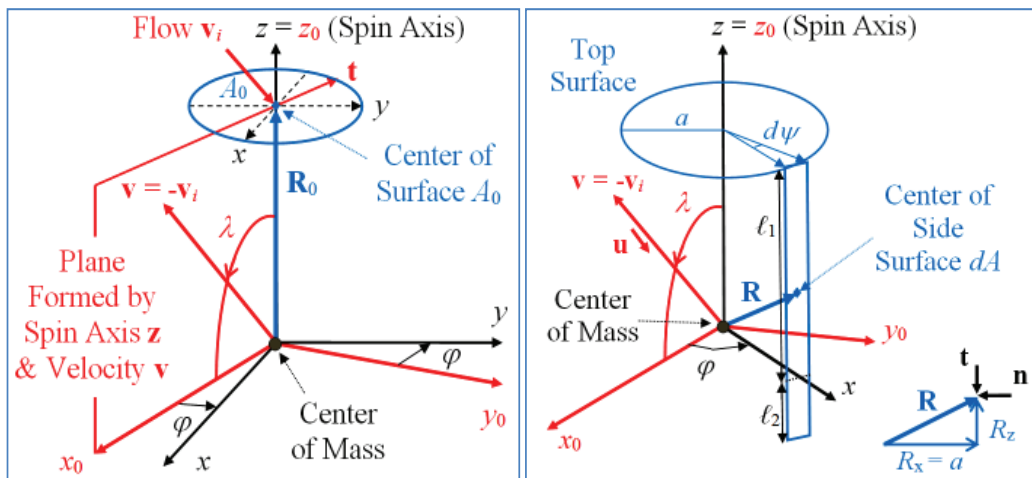
$$\mathbf{F} = \frac{1}{2} \rho v^2 A (C_n \mathbf{n} + C_t \mathbf{t}) \quad (17)$$

where v is the satellite's orbital velocity, which is taken identical to $-v_i$. The coefficients C_n and C_t are defined in Eqs. (14) and the unit-vectors \mathbf{n} and \mathbf{t} are defined by the geometry shown in Figure 1. Eq. (17) is consistent with previous results, for instance Eq. (28) of Reference 7, which has been derived by an alternative approach based on accommodation coefficients¹.

Next, we consider a flat surface element A as part of a satellite's external surfaces. In the calculation of the FMF torque exerted on surface A the knowledge of the lever arm \mathbf{R} in satellite body coordinates is needed. If the surface's FMF properties may be considered to be perfectly uniform or homogeneous, it follows from symmetry considerations that the FMF force acts at the geometrical center of surface A . Thus, the lever arm vector \mathbf{R} points from the satellite's center of mass to the geometrical center of surface A . The \mathbf{n} and \mathbf{R} vectors maintain their fixed orientations within the (rigid) spinning body frame. On the other hand, the incident velocity vector rotates relative to the spinning body frame. As a consequence, the FMF force may act over the whole or part of the spin period, or even not at all, depending on the surface's orientation with respect to the flow. Next, we evaluate the FMF effects on the top and side surfaces of a spinning satellite.

Disc-Shaped Top Surface

Figure 3a illustrates the disc-shaped top surface element A_0 as part of a cylindrical satellite configuration. The x_0, y_0, z_0 axes refer to the instantaneous reference frame defined by the spin-axis direction and the orbital velocity vector. Furthermore, the body-fixed x, y, z frame rotates about the $z = z_0$ axis with the instantaneous spin phase angle φ relative to the x_0 axis. The surface' FMF characteristics are considered uniform so the FMF force acts at the geometrical center of surface A_0 . The lever arm \mathbf{R}_0 points along the body's $+z$ -axis to the center of surface A_0 . Figure 3a shows that the flow velocity \mathbf{v}_i remains constant relative to the surface A_0 during the spin period.



Figures 3a,b. Geometrical Parameters of Surface Elements: Top (left) and Side Strip (right).

When comparing Figure 3a with the FMF geometry in Figure 1 it follows that the unit-normal \mathbf{n} points in the direction of the $-z_0$ axis and the unit-tangential vector \mathbf{t} points along the $-x_0$ axis. Therefore, Eq. (17) produces the following force result for the top surface:

$$\mathbf{F}_{top} = -\frac{1}{2} \rho v^2 A_0 (C_n \mathbf{z}_0 + C_t \mathbf{x}_0) \quad (18)$$

Since \mathbf{R}_0 points along the $z = z_0$ axis it is clear that the C_n term cannot produce a contribution to the torque. Thus, the torque acting on the top surface originates only from the C_t term:

$$\mathbf{M}_{top} = \mathbf{R}_0 \times \mathbf{F}_{top} = -\frac{1}{2} \rho v^2 A_0 R_0 C_t \mathbf{y}_0 = -\frac{1}{2} \rho v^2 A_0 R_0 \sigma_d \sin(2\lambda) \mathbf{y}_0 \quad (19)$$

where Eq. (14b) has been substituted. It can be confirmed that the same expression is also valid for a *square* or other symmetric top surface with identical surface area A_0 .

Infinitesimal Cylindrical Side Surface

Figure 3b shows a flat infinitesimal surface 'strip' $dA = a \ell d\psi$ (with $\ell = \ell_1 + \ell_2$) as part of a cylindrical shell with uniform or homogeneous FMF interactive properties. The surface element dA in Figure 3b is located at an arbitrary spin phase angle φ with rotation matrix:

$$\begin{pmatrix} x \\ y \end{pmatrix} = \begin{bmatrix} \cos \varphi & \sin \varphi \\ -\sin \varphi & \cos \varphi \end{bmatrix} \begin{pmatrix} x_0 \\ y_0 \end{pmatrix} \quad (20)$$

When comparing the geometrical configuration in Figure 3b with Figure 1 we find that the inward normal vector to the surface dA points along the negative x axis, i.e. $\mathbf{n} = -\mathbf{x}$. The unit-vector \mathbf{u} points along the incident flow and lies within the x_0, z_0 plane with components:

$$\mathbf{u} = -(\sin \lambda \mathbf{x}_0 + \cos \lambda \mathbf{z}_0) \quad (21)$$

The components of the vector \mathbf{u} in the x, y, z body coordinate frame are:

$$\mathbf{u} = u_x \mathbf{x} + u_y \mathbf{y} + u_z \mathbf{z} \quad (22a)$$

$$\text{with: } u_x = -\sin \lambda \cos \varphi; \quad u_y = \sin \lambda \sin \varphi; \quad u_z = -\cos \lambda \quad (22b-d)$$

Therefore, the dot-product $\mathbf{u} \cdot \mathbf{n}$ of the unit-vectors \mathbf{u} and \mathbf{n} is as follows:

$$\cos \vartheta = \mathbf{u} \cdot \mathbf{n} = -\mathbf{u} \cdot \mathbf{x} = \sin \lambda \cos \varphi \quad (23)$$

The geometry in Figure 3b indicates that the surface dA is only subjected to the free-molecular flow if the condition $\mathbf{u} \cdot \mathbf{n} > 0$ is satisfied. Since $0 < \lambda < \pi$, Eq. (23) yields the intuitive result:

$$\sin \lambda \cos \varphi > 0 \Rightarrow -\pi/2 < \varphi < \pi/2 \quad (24)$$

This shows that the interval over which the FMF force is active lasts half a spin revolution and is symmetric about the x_0 axis (i.e., centered at $\varphi = 0$ when the normal \mathbf{n} crosses the $-x_0$ axis).

The FMF force $d\mathbf{F}$ acting on the surface dA can in principle be calculated from its definition in Eq. (17). The expression for C_t in Eq. (14b) contains a $\sin \vartheta$ term which may be expressed in the angle φ by means of Eq. (23). Unfortunately, this approach generates a square-root of a trigonometric function in φ . This creates considerable difficulties in the subsequent integration over φ . Therefore, we carry out a reformulation of the force component vector $C_t \mathbf{t}$ in Eq. (17):

$$C_t \mathbf{t} = 2\sigma_d \cos \vartheta \{\sin \vartheta \mathbf{t}\} = 2\sigma_d (\mathbf{u} \cdot \mathbf{n}) \{\mathbf{u} - (\mathbf{u} \cdot \mathbf{n}) \mathbf{n}\} \quad (25)$$

where Eqs. (7,14b) have been employed. Eq. (25) leads to the modification of the force expression in Eq. (17), which is now written in its components along the unit-vectors \mathbf{n} and \mathbf{u} :

$$d\mathbf{F} = \frac{1}{2} \rho v^2 dA (C_n \mathbf{n} + C_t \mathbf{t}) = \frac{1}{2} \rho v^2 dA (\tilde{C}_n \mathbf{n} + C_u \mathbf{u}) \quad (26)$$

with:

$$\tilde{C}_n = C_n - 2\sigma_d (\mathbf{u} \cdot \mathbf{n})^2 = c_0 + c_1 (\mathbf{u} \cdot \mathbf{n}) + 4(1 - \sigma_d)(\mathbf{u} \cdot \mathbf{n})^2 \quad (27a)$$

$$C_u = 2\sigma_d (\mathbf{u} \cdot \mathbf{n}) \quad (27b)$$

The lever arm vector $\mathbf{R} = (R_x, 0, R_z)^T$ points from the center of mass to the geometrical center of surface dA as shown in Figure 3b. The vectors \mathbf{n} and \mathbf{R} maintain their fixed directions within the body frame, which spins about its z axis with spin phase angle φ relative to the inertial x_0, z_0 plane. The components of the torque vector $d\mathbf{M}$ along the body axes follow from Eq. (26):

$$d\mathbf{M} = \mathbf{R} \times d\mathbf{F} = \frac{1}{2} \rho v^2 dA \{\tilde{C}_n (\mathbf{R} \times \mathbf{n}) + C_u (\mathbf{R} \times \mathbf{u})\} \quad (28)$$

with:

$$\mathbf{R} \times \mathbf{n} = -R_z \mathbf{y} \quad (29a)$$

$$\mathbf{R} \times \mathbf{u} = -R_z u_y \mathbf{x} + (R_z u_x - R_x u_z) \mathbf{y} + R_x u_y \mathbf{z} \quad (29b)$$

The torque expressions in Eqs. (28-29) are valid for any spin phase angle φ within the interval $-\pi/2 < \varphi < \pi/2$, see Eq. (24). The torque vanishes outside this interval where the surface dA is not exposed to the FMF effects. The body components of the FMF torque $d\mathbf{M}$ acting on the surface dA follows by substituting the results of Eqs. (29a,b) into Eq. (28).

In order to be able to track the change in the angular momentum vector in inertial space, it is necessary to formulate the torque vector of Eq. (28) in *inertial* x_0, y_0, z_0 coordinates. Obviously, the vector \mathbf{u} is known in inertial coordinates from Eq. (21). The dot-product $\mathbf{u} \cdot \mathbf{n}$ is invariant to a coordinate transformation, so \mathbf{n} and \mathbf{R} are the remaining parameters to be transformed:

$$\mathbf{n} = -(\cos \varphi \mathbf{x}_0 + \sin \varphi \mathbf{y}_0); \quad \mathbf{R} = R_x (\cos \varphi \mathbf{x}_0 + \sin \varphi \mathbf{y}_0) + R_z \mathbf{z}_0 \quad (30a,b)$$

Eqs. (29) can be written in inertial x_0, y_0, z_0 coordinates by using the transformation in Eq. (20):

$$\mathbf{R} \times \mathbf{n} = -R_z (\cos \varphi \mathbf{y}_0 - \sin \varphi \mathbf{x}_0) \quad (31a)$$

$$\mathbf{R} \times \mathbf{u} = -R_x \cos \lambda \sin \varphi \mathbf{x}_0 + (R_x \cos \lambda \cos \varphi - R_z \sin \lambda) \mathbf{y}_0 + R_x \sin \lambda \sin \varphi \mathbf{z}_0 \quad (31b)$$

When substituting Eqs. (31) in Eq. (28) we obtain the FMF torque in *inertial* coordinates acting on the surface dA for an arbitrary phase angle φ in the interval $-\pi/2 < \varphi < \pi/2$.

Integrated Torque over Spin Period

In order to establish the net effective torque over the spin period we calculate the average value of the FMF torque $d\mathbf{M}$ on the surface element dA over a full spin revolution. This requires integrating the torque results from Eqs. (28, 31) over the relevant range of the phase angle φ :

$$\langle d\mathbf{M} \rangle = \frac{1}{2\pi} \int_{-\pi/2}^{\pi/2} \{d\mathbf{M}(\varphi)\} d\varphi = \frac{1}{2\pi} \int_{-\pi/2}^{\pi/2} \{\mathbf{R}(\varphi) \times d\mathbf{F}(\varphi)\} d\varphi \quad (32)$$

The dot-product $\mathbf{u} \cdot \mathbf{n}$, the coefficients C_n and C_u , as well as the cross-products involving the lever-arms, are all trigonometric functions of φ . A priori, we recognize that *odd* trigonometric functions of φ vanish after integration over the symmetric interval $-\pi/2 < \varphi < \pi/2$. As a consequence, the evaluation of the net average value of the torque over the spin revolution in Eq. (32) reduces to calculating the following four non-vanishing integrals:

$$\mathbf{N}_k = \frac{1}{2\pi} \int_{-\pi/2}^{\pi/2} (\mathbf{u} \cdot \mathbf{n})^k (\mathbf{R} \times \mathbf{n}) d\varphi \quad (k = 0, 1, 2) \quad (33a)$$

$$\mathbf{U} = \frac{1}{2\pi} \int_{-\pi/2}^{\pi/2} (\mathbf{u} \cdot \mathbf{n})(\mathbf{R} \times \mathbf{u}) d\varphi \quad (33b)$$

After substituting the expressions from Eqs. (23, 27, 31) into the integrands of Eqs. (33), it is fairly straightforward to obtain the following explicit results for these integrals:

$$\mathbf{N}_0 = -R_z I_1 \mathbf{y}_0; \quad \mathbf{N}_1 = -R_z I_2 (\sin \lambda) \mathbf{y}_0; \quad \mathbf{N}_2 = -R_z I_3 (\sin \lambda)^2 \mathbf{y}_0 \quad (34a-c)$$

$$\mathbf{U} = \sin \lambda (R_x I_2 \cos \lambda - R_z I_1 \sin \lambda) \mathbf{y}_0 \quad (34d)$$

where the integrals I_k ($k = 1, 2, 3$) are defined as:

$$I_k = \frac{1}{2\pi} \int_{-\pi/2}^{\pi/2} (\cos \varphi)^k d\varphi \quad (k = 1, 2, 3) \quad (35a)$$

with:

$$I_1 = \frac{1}{\pi}; \quad I_2 = \frac{1}{4}; \quad I_3 = \frac{2}{3\pi} \quad (35b-d)$$

Thus, the following results have now been established for the integrals in Eqs. (33-34):

$$\mathbf{N}_0 = -\frac{R_z}{\pi} \mathbf{y}_0; \quad \mathbf{N}_1 = -\frac{R_z}{4} \sin \lambda \mathbf{y}_0; \quad \mathbf{N}_2 = -\frac{2R_z}{3\pi} (\sin \lambda)^2 \mathbf{y}_0 \quad (36a-c)$$

$$\mathbf{U} = \sin \lambda \left(\frac{R_x}{4} \cos \lambda - \frac{R_z}{\pi} \sin \lambda \right) \mathbf{y}_0 \quad (36d)$$

Finally, the average torque result of Eqs. (28, 32) can be expressed in the results in Eqs. (36):

$$\langle d\mathbf{M} \rangle = \frac{1}{2} \rho v^2 dA \{ [c_0 \mathbf{N}_0 + c_1 \mathbf{N}_1 + 4(1 - \sigma_d) \mathbf{N}_2] + 2\sigma_d \mathbf{U} \} \quad (37)$$

Torque on Cylindrical Shell

The average torque acting on an open cylindrical shell (illustrated in Figure 4a) follows by integrating the result for the infinitesimal side surface strip given in Eq. (37) over the full cylinder shell. This is accomplished by simply integrating the angle $d\psi$ in Figure 3b from 0 to 2π :

$$\langle \mathbf{M}_{cyl} \rangle = \frac{1}{2} \rho v^2 (2\pi a\ell) \{ [c_0 \mathbf{N}_0 + c_1 \mathbf{N}_1 + 4(1 - \sigma_d) \mathbf{N}_2] + 2\sigma_d \mathbf{U} \} \Rightarrow \quad (38a)$$

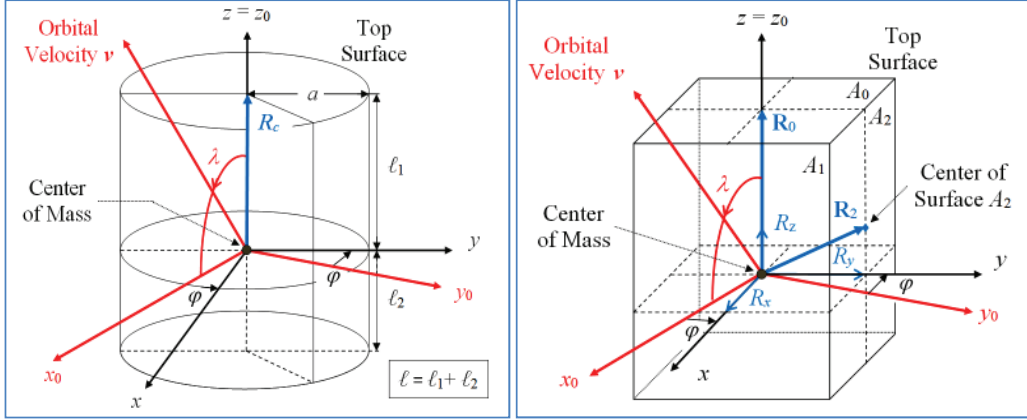
$$\boxed{\langle \mathbf{M}_{cyl} \rangle = -\frac{1}{2} \rho v^2 a\ell \left\{ (\ell_1 - \ell_2) \left[c_0 + c_1 \frac{\pi}{4} \sin \lambda + \frac{2}{3} (4 - \sigma_d) \sin^2 \lambda \right] - a \sigma_d \frac{\pi}{2} \sin(2\lambda) \right\} \mathbf{y}_0} \quad (38b)$$

where the results of Eqs. (36) and the lever arms $R_z = (\ell_1 - \ell_2)/2$ and $R_x = a$ have been substituted.

Box Side Surface

Figure 4b shows a box-shaped satellite with flat side surfaces A_1 and A_2 and flat top surface A_0 . All surfaces are assumed to have uniform or homogeneous FMF characteristics so the resulting FMF forces act at the geometrical centers of these surfaces. We focus on surface A_1 , whose orientation within the satellite's body-fixed frame is defined by the inward-pointing normal vector \mathbf{n}_1 . For simplicity (and without loss of generality) the normal \mathbf{n}_1 is taken to be pointing along the negative body x -axis, i.e. $\mathbf{n}_1 = (-1, 0, 0)^T$. Comparison with Figure 1 indicates that the tangential vector \mathbf{t}_1 points along the negative $z = z_0$ axis for incidence angles $0 < \lambda < \pi/2$.

The spin phase angle $\varphi = 0$ corresponds to the instant when the body-fixed x axis crosses the inertial x_0 axis, see Figure 4b. In general, the phase angle φ is non-zero and the vector \mathbf{n}_1 must be expressed in components along the instantaneous inertial (x_0, y_0, z_0) axes in a similar way as done in Eq. (30a). The FMF force \mathbf{F}_1 that acts on the surface A_1 follows from its definition in Eq. (17) and will remain active as long as the phase angle φ is within the interval $-\pi/2 < \varphi < \pi/2$. Identical considerations hold of course for the surface A_2 with its normal \mathbf{n}_2 and its FMF force \mathbf{F}_2 .



Figures 4a,b. Definition of Parameters for Cylindrical (left) and Box-Like Configurations (right).

The lever arm vector points from the center of mass to the geometrical center of surface \$A_1\$ and is given by \$\mathbf{R}_1 = (R_x, 0, R_z)^T\$. Similarly, for surface \$A_2\$ we have \$\mathbf{R}_2 = (0, R_y, R_z)^T\$, see Figure 4b. The vectors \$\mathbf{R}_j (j = 1, 2)\$ can be written in their inertial \$(x_0, y_0, z_0)\$ components similarly as was done in Eq. (30b). As before, the vectors \$\mathbf{n}_j\$ and \$\mathbf{R}_j\$ maintain their fixed directions within the body frame, which rotates with spin phase angle \$\varphi\$ about the \$z_0\$ axis of the inertial frame.

The torque expressions follow as in Eqs. (28) but are already integrated over the surfaces \$A_j\$:

$$\mathbf{M}_j = \mathbf{R}_j \times \mathbf{F}_j = \frac{1}{2} \rho v^2 A_j \{ \tilde{C}_{nj} (\mathbf{R}_j \times \mathbf{n}_j) + C_{uj} (\mathbf{R}_j \times \mathbf{u}) \} \quad (j=1,2) \quad (39)$$

After expressing the two cross-products appearing in Eqs. (39) in their components along the \$(x_0, y_0, z_0)\$ axes similarly as was done in Eqs. (31) and employing the integrals defined in Eqs. (33), we obtain similar average torque results as in Eqs. (32–37) for the surfaces \$A_j\$ with \$j = 1, 2\$:

$$\langle \mathbf{M}_j \rangle = \langle \mathbf{R}_j \times \mathbf{F}_j \rangle = \frac{1}{2} \rho v^2 A_j \{ [c_0 \mathbf{N}_0 + c_1 \mathbf{N}_1 + 4(1 - \sigma_d) \mathbf{N}_2] + 2\sigma_d \mathbf{U} \} \Rightarrow \quad (40a)$$

$$\boxed{\langle \mathbf{M}_j \rangle = -\frac{1}{2} \rho v^2 A_j \left\{ R_z \left[\frac{c_0}{\pi} + \frac{c_1}{4} \sin \lambda + \frac{2}{3\pi} (4 - \sigma_d) \sin^2 \lambda \right] - R_{x/y} \frac{\sigma_d}{4} \sin(2\lambda) \right\} \mathbf{y}_0} \quad (40b)$$

The total torque acting on an open box-shaped satellite consisting of 4 identical rectangular side surfaces follows immediately from the result in Eq. (40b) by simply multiplying it by 4.

Idealized Satellite Configurations

Figures 4a,b show two idealized satellite configurations, i.e. a cylinder and a rectangular box. The average FMF torques can be obtained by adding the individual torque results for the surface elements given above. For a satellite consisting of a cylindrical shell plus a circular disk as top surface, the average torque contributions over the spin period follow from Eqs. (19, 38b):

$$\langle \mathbf{M}_{top} \rangle = \mathbf{M}_{top} = -\frac{1}{2} \rho v^2 A_{top} R_0 \sigma_d \sin(2\lambda) \mathbf{y}_0 \quad (41a)$$

$$\langle \mathbf{M}_{cyl} \rangle = -\frac{1}{2} \rho v^2 a \ell \left\{ (\ell_1 - \ell_2) \left[c_0 + \frac{\pi}{4} c_1 \sin \lambda + \frac{2}{3} (c_2 + \sigma_d) \sin^2 \lambda \right] - a \sigma_d \frac{\pi}{2} \sin(2\lambda) \right\} \mathbf{y}_0 \quad (41b)$$

where the geometrical parameters are defined in Figure 4a.

In the case $\lambda > \pi/2$, the lever arm vector \mathbf{R}_0 points to the center of the *bottom* surface as the incident FMF interacts with the bottom surface. This situation would lead to a change of sign for the torque in Eq. (41a). However, it must be recognized that (in non-trivial problems) also the length $|\mathbf{R}_0|$ changes abruptly when λ passes through $\pi/2$, so the results would be discontinuous. In order to avoid sign and interpretation issues, it is recommended to work only with $\lambda \leq \pi/2$. The cylinder must thus be turned ‘upside down’ for $\pi/2 < \lambda \leq \pi$ to obtain the geometry of Figure 4a.

Likewise, the average torques over the spin period can be established for the box-like satellite shown in Figure 4b with top surface A_0 and (in general) different side surfaces A_1 and A_2 . The contribution of the top surface A_0 is identical to the result for the cylinder given in Eq. (41a). The average FMF torque acting on the four side surfaces follows readily from Eq. (40b). The total average torque acting on the box (including the contribution of the top surface) is given by:

$$\langle \mathbf{M}_{\text{box}} \rangle = -\frac{1}{2} \rho v^2 \left\{ (A_1 + A_2) \frac{R_z}{\pi} \left[2c_0 + \frac{\pi}{2} c_1 \sin \lambda + \frac{2}{3} (c_2 + \sigma_d) \sin^2 \lambda \right] - \frac{1}{2} D \sigma_d \sin(2\lambda) \right\} \mathbf{y}_0 \quad (42a)$$

with:

$$D = (A_1 R_x + A_2 R_y - 2A_0 R_z) \quad (42b)$$

Finally, it may be noted that, for regular symmetric satellite configurations, the FMF torque can be expected to act along the $\pm \mathbf{y}_0$ axis, i.e. normal to the plane defined by the velocity vector and the spin-axis attitude. Its sign follows from the relative magnitudes of the force components in Eqs. (18). It has been negative for all example configurations considered here.

Generic Torque Expressions

Here, we present a generic expression for the spin-averaged FMF torque that covers the results for the cylindrical as well as box-like spinning satellite configurations quoted above. This result may be considered representative for an arbitrary symmetrical or regular satellite configuration:

$$\langle \mathbf{M} \rangle = -\frac{1}{2} \rho v^2 \{ C_0 + \sin \lambda [C_1 + C_2 \sin \lambda + C_3 \cos \lambda] \} \mathbf{y}_0 \Rightarrow \quad (43a)$$

$$\boxed{\langle \mathbf{M} \rangle = -\frac{1}{2} \rho (\mathbf{z} \times \mathbf{v}) \{ C_0 v^2 / |\mathbf{z} \times \mathbf{v}| + C_1 v + C_2 |\mathbf{z} \times \mathbf{v}| + C_3 (\mathbf{z} \cdot \mathbf{v}) \}} \quad (43b)$$

where λ is defined as the angle between the orbital velocity vector \mathbf{v} and the spin-axis attitude unit-vector \mathbf{z} and is assumed to be within the range $(0, \pi/2)$. For values of $\lambda > \pi/2$, the top surface becomes the bottom surface and vice versa, as discussed in the previous section.

The coefficients C_j ($j = 0, 1, \dots, 3$) in Eqs. (43) contain the satellite’s geometrical as well as the FMF parameters. For illustration, Table 1 summarizes the expressions for the parameters C_j in the case of the box-like and cylindrical satellites for which the results were given in Eqs. (41-42).

In the analytical model presented here, the satellite’s body frame is considered ‘frozen’ (i.e., inertially-fixed) throughout the spin revolution. The attitude change induced by the FMF torque is taken into account at the end of each spin revolution. At that time, the body frame is updated or rectified on the basis of the calculated attitude change experienced over the previous spin period. This procedure is justified as long as the attitude changes over a spin period are ‘infinitesimal’. In practice, this condition is guaranteed because the spin period is extremely short (of the order of a second) relative to the interval of 10 to 15 minutes over which the attitude change is generated.

Table 1. Parameters C_j ($j = 0, \dots, 3$) for Box-Like and Cylindrical Satellite Configurations.

Parameters [m^3]	Box	Cylinder (Shell)
C_0	$2(A_1 + A_2)R_z c_0 / \pi$	$a(l_1^2 - l_2^2)c_0$
C_1	$R_z(A_1 + A_2)c_1 / 2$	$a(l_1^2 - l_2^2)c_1\pi/4$
C_2	$4R_z(A_1 + A_2)(c_2 + \sigma_d)/(3\pi)$	$2a(l_1^2 - l_2^2)(c_2 + \sigma_d)/3$
C_3	$(2A_0 R_0 - A_1 R_x - A_2 R_y)\sigma_d$	$\pi a^2(2R_0 - \ell)\sigma_d$

CHANGE IN SPIN-AXIS ATTITUDE VECTOR

Orbit Model

The satellite's velocity vector is written in terms of the eccentric anomaly E . Its components along the perigee coordinate axes with (vertical, horizontal) unit vectors ξ_p, η_p are as follows:

$$\mathbf{v}(E) = \sqrt{\mu/a} \left\{ -\sin E \xi_p + s_e \cos E \eta_p \right\} / (1 - e \cos E) \quad (44)$$

where a is the semi-major axis, e denotes the eccentricity, $s_e = \sqrt{1-e^2}$, and $\mu = 3.986 \times 10^{14} \text{ m}^3/\text{s}^2$ is the Earth's gravitational parameter. The magnitude of the velocity vector is:

$$v(E) = \sqrt{\frac{\mu}{a} \left(\frac{1+e \cos E}{1-e \cos E} \right)} \quad (45)$$

The atmospheric density is given by the straightforward exponential model (see King-Hele¹²):

$$\rho(E) = \rho_p \exp \left\{ -[r(E) - r_p] / H_p \right\} = \rho_p \exp \left\{ -\beta(1 - \cos E) \right\} \quad (46)$$

where ρ_p and H_p denote the density and its scale height at the perigee position r_p , respectively. The non-dimensional parameter β is defined by:

$$\beta = ae / H_p \quad (47)$$

When substituting, for instance, the relevant data of the MARECS-A GTO, i.e. $a \approx 2.44 \times 10^4$ km, $e \approx 0.73$, $H_p \approx 33$ km, we obtain $\beta \approx 540$, which may be considered typical for a GTO. The density reaches its maximum value at the perigee position r_p and diminishes very rapidly away from the perigee. At $E = \pm 7.5^\circ$, which correspond to only ± 3.6 minutes away the perigee location, the density levels are already below 1 % of the density at the perigee. Therefore, it is justified to neglect the torque contributions further away from the perigee region.

Change in Angular Momentum Vector

First, the spin axis attitude vector is transformed from its inertial representation $\mathbf{z} = (z_1, z_2, z_3)^\top$ to its components $(z_\xi, z_\eta, z_\zeta)^\top$ along the perigee reference frame (see visualization in Figure 5):

$$\mathbf{z} = z_\xi \xi_p + z_\eta \eta_p + z_\zeta \zeta_p \quad (48a)$$

with:

$$z_\xi = \sin \lambda_p \cos \mu_p; \quad z_\eta = \cos \lambda_p; \quad z_\zeta = \sin \lambda_p \sin \mu_p \quad (48b-d)$$

The spin-axis \mathbf{z} is assumed to remain inertially-fixed during the short interval around perigee. Thus, the cone and clock angles λ_p, μ_p are constants in the perigee reference frame (ξ_p, η_p, ζ_p) .

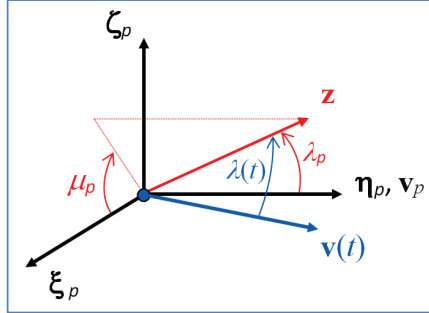


Figure 5. Definitions of Cone and Clock Angles λ_p, μ_p .

The terms of torque vector in Eq. (43b) are expressed as functions of the eccentric anomaly E :

$$\mathbf{z} \cdot \mathbf{v}(t) = v \cos \lambda(t) = \sqrt{\mu/a} (z_\eta s_e \cos E - z_\xi \sin E) / (1 - e \cos E) \quad (49a)$$

$$\mathbf{z} \times \mathbf{v}(t) = \sqrt{\mu/a} \{ s_e \cos E (\mathbf{z} \times \boldsymbol{\eta}_p) - \sin E (\mathbf{z} \times \boldsymbol{\xi}_p) \} / (1 - e \cos E) \quad (49b)$$

$$|\mathbf{z} \times \mathbf{v}(t)| = v \sin \lambda(t) = \sqrt{v^2 - (\mathbf{z} \cdot \mathbf{v})^2} = \sqrt{\mu/a} f(E) / (1 - e \cos E) \quad (49c)$$

with:

$$f(E) = \left\{ 1 - e^2 \cos^2 E - (z_\eta s_e \cos E - z_\xi \sin E)^2 \right\}^{1/2} \quad (49d)$$

The generic average torque in Eq. (43b) can now be expressed as a function of E :

$$\langle \mathbf{M}(E) \rangle = -\frac{1}{2} \rho_p \left(\frac{\mu}{a} \right) \frac{F(E)}{(1 - e \cos E)^2} \{ s_e \cos E (\mathbf{z} \times \boldsymbol{\eta}_p) - \sin E (\mathbf{z} \times \boldsymbol{\xi}_p) \} \exp[-\beta(1 - \cos E)] \quad (50)$$

with:

$$F(E) = C_0 (1 - e^2 \cos^2 E) / f(E) + C_1 \sqrt{1 - e^2 \cos^2 E} + C_2 f(E) + C_3 (z_\eta s_e \cos E - z_\xi \sin E) \quad (51)$$

The change $\Delta \mathbf{H}$ in the satellite's rotational angular momentum vector $\mathbf{H} = I_z \mathbf{z}$ (with I_z the axial moment of inertia) follows by integrating the torque vector in Eq. (50) over the perigee region:

$$\Delta \mathbf{H} = \int_{t_p - t_1}^{t_p + t_1} \langle \mathbf{M}(t) \rangle dt = \sqrt{(a^3 / \mu)} \int_{-E_1}^{+E_1} \langle \mathbf{M}(E) \rangle (1 - e \cos E) dE \quad (52)$$

Because the integration interval is symmetric about the perigee position $E = 0$, odd functions of E do not contribute to the integral in Eq. (52). Thus, only even terms of the torque in Eq. (50) need to be taken into account. After collecting the contributing terms, Eq. (52) becomes:

$$\Delta \mathbf{H} = -\rho_p \sqrt{\mu a} \{ (\mathbf{z} \times \boldsymbol{\eta}_p) J_1(E_1) - (\mathbf{z} \times \boldsymbol{\xi}_p) J_2(E_1) \} \quad (53)$$

The integrals $J_m(E_1)$, $m = 1, 2$ originate from the results in Eqs. (50) and (52) and are defined as:

$$J_m(E_1) = \int_{-E_1}^{E_1} G_m(E) \exp[-\beta(1 - \cos E)] dE \quad (m=1,2) \quad (54)$$

where $G_m(E)$ are the surviving even functions of E in the integrand of Eq. (52) in units of $[m^3]$.

The integrals in Eq. (54) can be simplified by using the integration variable $u = \sqrt{(1 - \cos E)}$ and subsequently expanding the functions $G_m[E(u)]$, $m = 1, 2$, in power series in the variable u .

Since the parameter β is large (see Eq. 47 and accompanying text), the exponential term in Eq. (54) obtains its major contributions from a small region centered at the perigee. Application of the Laplace Method (see Bender et al.¹³) to the integrals in Eq. (54) with integration variable u and large parameter β leads to the compact asymptotic result for $\Delta\mathbf{H}$ in Eq. (53), see van der Ha⁸:

$$\Delta\mathbf{H} \approx -\rho_p \sqrt{\frac{2\pi\mu a}{\beta}} \left\{ \gamma_{10}(\mathbf{z} \times \boldsymbol{\eta}_p) + \frac{1}{2\beta} [\gamma_{11}(\mathbf{z} \times \boldsymbol{\eta}_p) - \gamma_{21}(\mathbf{z} \times \boldsymbol{\xi}_p)] + O\left(\frac{1}{\beta^2}\right) \right\} \quad (55)$$

where the coefficients γ_{mk} ($m = 1, 2$; $k = 0, 1$) are associated with $G_m[E(u)]$ and with the powers of the asymptotic power series in $(1/\beta)^{k+1/2}$, respectively. The two coefficients for $k = 0$ represent the leading terms of the asymptotic expansion in Eq. (55) and are defined as:

$$\gamma_{10} = (1+e)\{C_0 / \sin \lambda_p + C_1 + C_2 \sin \lambda_p + C_3 z_\eta\}; \quad \gamma_{20} = 0 \quad [m^3] \quad (56a-b)$$

The term containing [...] in Eq. (55) is of the order of $(1/\beta)^{3/2}$, which amounts to about 0.2 % of the leading term γ_{10} (for GTO applications). Therefore, this term safely be neglected.

Change in Spin-Axis Direction

After nutation effects subside, the coordinates of the updated (i.e., after passage of the perigee region) spin-axis attitude vector \mathbf{z}^+ in the perigee reference frame follow from $\Delta\mathbf{H}$ in Eq. (55):

$$\mathbf{z}^+ = \mathbf{z}^- + \Delta\mathbf{z} \approx (z_\xi + \varepsilon z_\zeta) \boldsymbol{\xi}_p + z_\eta \boldsymbol{\eta}_p + (z_\zeta - \varepsilon z_\xi) \boldsymbol{\zeta}_p \quad (57a)$$

$$\Rightarrow \Delta\mathbf{z} \approx \varepsilon z_\zeta \boldsymbol{\xi}_p - \varepsilon z_\xi \boldsymbol{\zeta}_p = \varepsilon \sin \lambda_p (\sin \mu_p \boldsymbol{\xi}_p - \cos \mu_p \boldsymbol{\zeta}_p) \quad (57b)$$

with:

$$\varepsilon = \frac{\Delta H}{H} \approx \gamma_{10} \rho_p \frac{1}{H} \sqrt{\frac{2\pi\mu a}{\beta}} \quad [rad] \quad (57c)$$

The result in Eqs. (57b) indicates that the magnitude of the spin-axis attitude change is:

$$|\Delta\mathbf{z}| \approx \varepsilon |\boldsymbol{\eta}_p \times \mathbf{z}| \approx \varepsilon \sin \lambda_p \quad (58a,b)$$

As expected, the orientation angle λ_p between the perigee velocity vector and the spin-axis has a significant influence on the change in the attitude vector under the FMF torque.

Because of the dominance of the torque vector in the perigee region, the vectors $\Delta\mathbf{H}$ and $\Delta\mathbf{z}$ (i.e., changes in angular momentum vector as well as in attitude direction) point along the vector $\mathbf{z} \times \boldsymbol{\eta}_p$ as indicated by the leading term in Eq. (55). During the satellite passage through the perigee region, the spin axis \mathbf{z} has moved by the angle $\varepsilon \sin \lambda_p$ along the cone with cone angle λ_p from the $\boldsymbol{\eta}_p$ axis, see also Figure 5. In accordance with the well known gyroscopic effect, the direction of the spin-axis change is along the applied torque vector \mathbf{M} and the resulting $\Delta\mathbf{H}$ vector.

Next, the result of Eq. (57b) is transformed to inertial components. First, the perigee frame is transformed to the inertial frame by means of the rotation matrix A :

$$\begin{pmatrix} \boldsymbol{\xi}_p \\ \boldsymbol{\eta}_p \\ \boldsymbol{\zeta}_p \end{pmatrix} = A \begin{pmatrix} X \\ Y \\ Z \end{pmatrix}; \text{ with: } A = \begin{pmatrix} c_\omega c_\Omega - s_\omega s_\Omega c_i & c_\omega s_\Omega + s_\omega c_\Omega c_i & s_\omega s_i \\ -s_\omega c_\Omega - c_\omega s_\Omega c_i & -s_\omega s_\Omega + c_\omega c_\Omega c_i & c_\omega s_i \\ s_\Omega s_i & -c_\Omega s_i & c_i \end{pmatrix} \quad (59a,b)$$

where c_x and s_x denote $\cos(x)$ and $\sin(x)$, respectively. When substituting the expression for the $\boldsymbol{\eta}_p$ axis in Eq. (58a) we obtain the components of $\Delta\mathbf{z} = \{\Delta z_1, \Delta z_2, \Delta z_3\}$ in inertial coordinates:

$$\Delta \mathbf{z} \equiv \varepsilon |\mathbf{\eta}_p \times \mathbf{z}| \Rightarrow \Delta \mathbf{z}_{inertial} = \begin{pmatrix} \Delta z_1 \\ \Delta z_2 \\ \Delta z_3 \end{pmatrix} \equiv \varepsilon \begin{pmatrix} z_3 A_{22} - z_2 A_{23} \\ z_1 A_{23} - z_3 A_{21} \\ z_2 A_{21} - z_1 A_{22} \end{pmatrix} \quad (60)$$

with A_{jk} ($j, k = 1, 2, 3$) referring to the entries in the matrix A of Eq. (59b).

The changes in the attitude's right ascension and declination angles α, δ are as follows:

$$\mathbf{z} = (z_1, z_2, z_3)^T = (\cos \alpha \cos \delta, \sin \alpha \cos \delta, \sin \delta)^T \Rightarrow \quad (61a)$$

$$\Delta \alpha = (\Delta z_2 \cos \alpha - \Delta z_1 \sin \alpha) / \cos \delta = \varepsilon \left\{ c_\omega s_i + (s_\omega c_{\alpha-\Omega} - c_\omega s_{\alpha-\Omega} c_i) \tan \delta \right\} \quad (61b)$$

$$\Delta \delta = -\Delta z_3 / \cos \delta = -\varepsilon \left\{ s_\omega s_{\alpha-\Omega} + c_\omega c_{\alpha-\Omega} c_i \right\} \quad (61c)$$

When comparing these results with Eq. (58), it follows that the total attitude change is given by:

$$|\Delta \mathbf{z}| = \sqrt{(\Delta \delta)^2 + \cos^2 \delta (\Delta \alpha)^2} = \varepsilon \sin \lambda_p \quad (62)$$

Finally, the solar aspect angle ϑ is defined as $\arccos(\mathbf{z} \cdot \mathbf{s})$ where \mathbf{s} stands for the Sun direction seen from the satellite with instantaneous inertial coordinates $\mathbf{s} = (s_1, s_2, s_3)^T$. Small changes in the attitude vector produce similarly small changes in the observed Sun aspect angle:

$$\Delta \vartheta = -(\Delta \mathbf{z}) \cdot \mathbf{s} / \sin \vartheta = c_\alpha \Delta \alpha + c_\delta \Delta \delta \quad (63)$$

The coefficients c_α and c_δ can readily be expressed in the attitude and Sun vector components.

DISCUSSION OF RESULTS

Simulations have been performed to enhance our understanding of the dependence of the torque characteristics and the associated attitude changes on the applicable input parameters, in particular: perigee altitude, atmospheric density and scale height parameters, angle between the satellite spin axis and perigee velocity, satellite geometrical configuration parameters, and characteristics of the free-molecular and satellite surface interactions.

Figures 6a,b show the normalized FMF torque $\mathbf{M}/(\rho v^2/2)$ in the $-y_0$ direction as function of the incidence angle λ over the range $(0, \pi/2)$ with input parameters summarized in Table 2. In Figure 6a, the center of pressure position R_z is *above* the center of mass and in Figure 6b it is *below*. The direction of the torque induced by the top surface is unchanged but its magnitude varies due to the different lever arms in Figures 6a,b. The forces acting on the cylindrical shell are separated in their normal and tangential components according to Eqs. (14a,b). Figures 6a,b indicate that, the sign change of the center of pressure inverts the torque direction of the normal forces. The tangential forces have the cylinder radius as their lever arms so their torques remain unchanged.

Table 2. Input Parameters for Cylindrical Satellite Configurations in Figures 6a,b.

Geometry Figures 6a	Geometry Figure 6b	Free-Molecular Flow
$a = 0.913$ m		$v_i = 10.2$ km/s
$\ell_1 = 1.192$ m	$\ell_1 = 0.762$ m	$v_m = 950$ m/s
$\ell_2 = 0.762$ m	$\ell_2 = 1.192$ m	$T_w/T_m = 0.3$
$R_z = +0.215$ m	$R_z = -0.215$ m	$\sigma_d = 1.0$

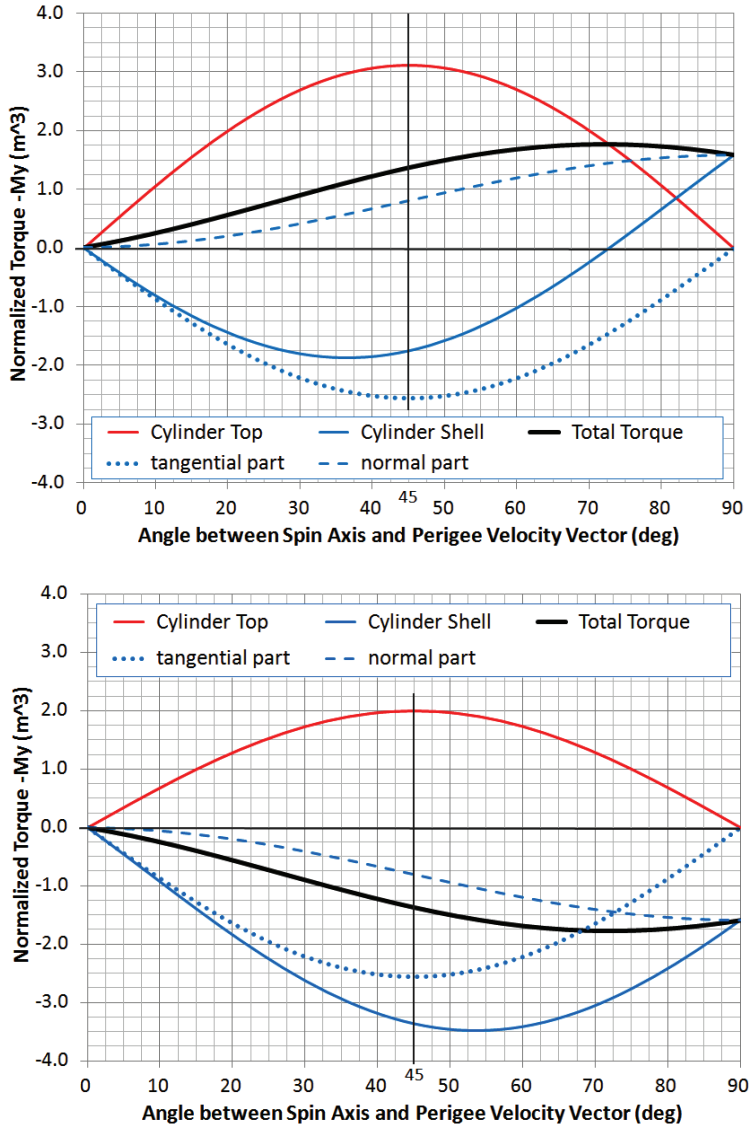


Figure 6. Normalized Torques on Cylindrical Body: (a) $R_z = +0.214 \text{ m}$; (b) $R_z = -0.214 \text{ m}$.

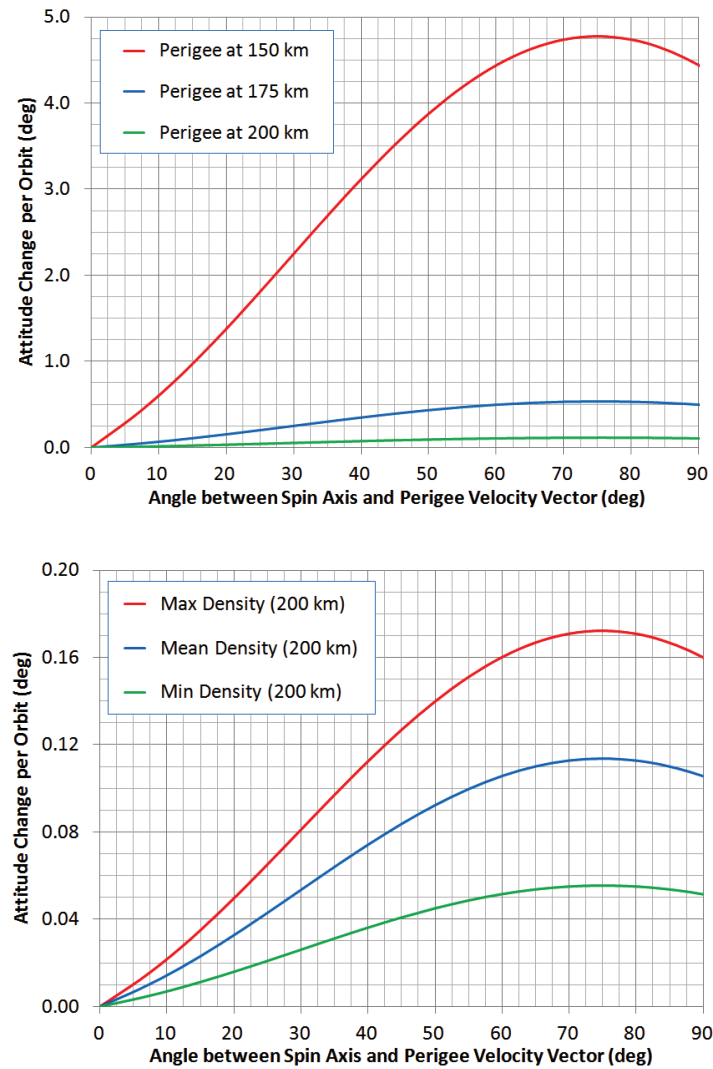
Figures 7a,b illustrate the attitude changes resulting from FMF torques acting on a box-like satellite for different perigee and density parameters, respectively. The input data are provided in Table 3. They correspond to the MARECS-A satellite configuration and orbit parameters during its GTO in December 1981 (van der Ha^{7,8}). The data for the density and scale heights are taken from Wertz et al.¹⁴. These are not the actual values experienced by MARECS-A at the time but they are more suitable for the general mission analysis pursued in Figures 7a,b.

Figure 7a shows the dependence of the FMF-induced attitude change on the perigee altitude for three cases in the range from 150 to 200 km. The maximum attitude change over the perigee region occurs when the attitude orientation is about 75 degrees from the perigee velocity vector. It can be seen that the maximum change varies from 0.15° to 4.8° depending on the perigee height.

Table 3. Input Data for Box-Like Satellite Configuration and Perigee Altitude Range 200 - 150 km.

Geometry	Orbit	Density	Attitude	Free-Molecular
$R_x = 0.809 \text{ m}$	$a = 24363 \text{ km}$	$\rho_p = 2.4 - 17.3 \times 10^{-10} \text{ kg/m}^3$	$I_z = 352.7 \text{ kg m}^2$	$v_i = 10.2 \text{ km/s}$
$R_y = 0.809 \text{ m}$	$e = 0.73$	$H_p = 37.5 - 25.5 \text{ km}$	$H = 2412 \text{ N m s}$	$v_m = 950 \text{ m/s}$
$R_z = 0.215 \text{ m}$	$\omega, \Omega = 174.8^\circ, 273.7^\circ$	$\beta = ae/H_p = 474 \text{ to } 692$	$\Omega_{\text{spin}} = 65.3 \text{ rpm}$	$T_w / T_m = 0.3$
$R_0 = 0.762 \text{ m}$	$i = 10.565^\circ$		$\lambda_p = 162.6^\circ$	$\sigma_d = 1.0$

Figure 7b illustrates the dependence of the attitude change on the atmospheric density for an orbit with 200-km perigee altitude in all cases. The results indicate that the low and high density conditions lead to a difference of a factor 3 in the maximum attitude change over the perigee.



Figures 7. Attitude Changes over Perigee for Different: (a) Perigee Heights; (b) Density Values.

CONCLUSIONS

The interactions of the free-molecular flow with a satellite surface in the perigee region of an elliptical Earth orbit has been investigated on the basis of the molecular velocity distributions predicted by Maxwell-Boltzmann's kinetic gas theory. The resulting forces acting on the satellite are derived from an aerodynamic model that incorporates diffuse molecular re-emissions as well as specular molecular reflections off the surface. Analytical expressions for the forces and torques induced by the free-molecular flow are calculated for idealized, but realistic, cylindrical and box-like satellite configurations. The resulting change in the satellite rotational angular momentum vector is established by integrating the torque vector over the perigee region as the contributions from the higher-altitude lower-density regions of the orbit are negligible. The change in angular momentum vector is determined in the form of an asymptotic series in the small parameter $1/\beta = H_p/(ae)$ with H_p the density scale height at perigee, a the semi-major axis, and e the eccentricity. This leads to explicit analytical results for the changes in the spin-axis attitude orientation under free-molecular flow effects. Finally, the analytical results are evaluated for their dependence on variations in the values of the perigee altitudes and atmospheric density values.

REFERENCES

- ¹ S.A. Schaaf and P.L. Chambre, "Flow of Rarefied Gases." *Princeton University Press*, 1961.
- ² G.E. Cook, "Satellite Drag Coefficients." *Planetary Space Science Review*, Vol. 13, October 1965, pp. 929-946.
- ³ G. Koppenwallner, "Freimolekulare Aerodynamik für Satellitenanwendung." *DFVLR FB-82-08, Deutsche Forschungs- und Versuchsanstalt für Luft- und Raumfahrt*, Göttingen, Germany, January 1982.
- ⁴ R.D. Boettcher and H. Legge, "Determination of Aerodynamic Forces on Satellites by Theory and Wind Tunnel Experiments." *Acta Astronautica*, Vol. 7, No. 4/5, April-May 1980, pp. 255-267.
- ⁵ R.D. Boettcher, "Analysis of Free Molecular Effects on the Attitude of Satellites in Geostationary Transfer Orbit; Part I: Theoretical Analysis." *DFVLR IB-222-86-A-08, Deutsche Forschungs- und Versuchsanstalt für Luft- und Raumfahrt*, Göttingen, Germany, 1986; also: ESA-CR(P) 2408, 1986.
- ⁶ G. Koppenwallner and H. Legge, "Analysis of Free Molecular Effects on the Attitude of Satellites in Geostationary Transfer Orbit; Part II: Force and Torque Measurement in Free Molecular Wind Tunnel Tests." *DFVLR IB-222-86-A-07, Deutsche Forschungs- und Versuchsanstalt für Luft- und Raumfahrt*, Göttingen, Germany, 1986; also: ESA-CR(P) 2408, 1986.
- ⁷ J. C. van der Ha, "Approximate Free-Molecular Flow Torques on Spinning Satellites." *The Journal of the Astronautical Sciences*, Vol. 34, No. 4, October-December 1986, pp. 403-419.
- ⁸ J. C. van der Ha, "Attitude Perturbations Induced by Free-Molecular Flow Interactions in Perigee Region." *Acta Astronautica*, Vol. 13, No. 6/7, June-July 1986, pp. 301-309.
- ⁹ H. Klinkrad and B. Fritsche, "Orbit and Attitude Perturbations due to Aerodynamics and Radiation Pressure." *ESA Workshop on Space Weather, ESA-WPP-155*, 11-13 November 1998, ESA / ESTEC, Noordwijk, the Netherlands.
- ¹⁰ V.L. Pisacane, "The Space Environment and its Effects on Space Systems, Chapter 7: The Neutral Environment." *American Institute of Aeronautics and Astronautics*, Reston, VA, 2008.
- ¹¹ K. Moe and M.M. Moe, "Gas-surface Interactions and Satellite Drag Coefficients." *Planetary and Space Sciences*, Vol. 53, Nr. 8, July 2005, pp. 793-801.
- ¹² D. King-Hele, "Theory of Satellite Orbits in an Atmosphere." *Butterworths*, London, 1964.
- ¹³ C.M. Bender and S.A. Orszag, "Advanced Mathematical Methods for Scientists and Engineers." *McGraw-Hill*, New York, 1978, p. 263.
- ¹⁴ J.A. Wertz and W.L. Larson, Eds., "Space Mission Analysis and Design, 3-rd Edition." *Microcosm / Springer*, 1999.